DESIGN AND INVESTIGATION OF A MULTISTAGE AXIAL CONTRA-ROTATING FAN

Christian FRIEBE[1], Oliver VELDE[2],
Ralph KRAUSE[1], Karsten HACKESCHMIDT[1]

[1] *INSTITUTE FÜR LUFT- UND KÄLTETECHNIK gGmbH, Bertolt-Brecht-Allee 20, 01309 Dresden, Germany*

[2] *CFTURBO GmbH, Unterer Kreuzweg 1, 01097 Dresden, Germany*

SUMMARY

The development of a multistage axial fan using contra-rotating wheels at each stage is described here. The outer diameter of the fan is 120 mm and the rotational speed for the first and the second impeller are 133.3 s^{-1} and 83.3 s^{-1}, respectively. The design of the complete fan is based upon the design approach for contra-rotating axial fans of CFturbo [12]. The first impeller was designed for a performance of 2/3 of the overall power. Hence, it was not necessary to fulfill the balancing of momentum although that is an available design option in CFturbo [12] amongst others. The contra-rotating axial fan is examined with different methods. Performance measurements and measurements on the velocity profile with optical methods (PIV) are provided to understand the working principle of every stage. The high efficiency and the axial outlet flow without tangential velocity components (swirl) are demonstrated with these measurements.

INTRODUCTION

Contra-rotating axial fans are investigated since the 1930s [5-6, 8]. Due to increasing efficiency demands and power density enhancement this technology is in focus since a short time again [9-11].

Axial blowing fans are common in many fields of application. By using an axial fan it should be noted there is a swirl occurring at the trailing edge of the blades due to the working principle. The swirl is not needed in most cases and may have unfavourable influence on subsequent devices, e.g. higher pressure drop or lower heat transfer coefficient. As the static pressure rise is an evaluation criterion for the fan efficiency there are different possibilities for converting the dynamic pressure of the swirl into a static pressure rise. The most common application for rising the efficiency is the installation of outlet guide vanes.

Contra-rotating axial fans (CRF) are well known as one opportunity to increase the efficiency of a fan, too. The efficiency increase is driven by the conversion of the dynamic pressure of the swirl at the trailing edge of the first axial fan blades into a static pressure at the end of the whole stage. In comparison with fans using discharge guide vanes, a higher power density can be obtained.

WORKING PRINCIPLE

Due to the Euler equation the specific work Y is defined by

$$Y = u'' c_u'' - u' c_u'. \tag{1}$$

For an axial fan stage obviously $u'' = u' = u$, wich transforms eq. (1) to

$$Y = u(c_u'' - c_u'). \tag{2}$$

With u as the amount of the peripheral speed, c_u as the component of the absolute fluid velocity vector $\boldsymbol{c}$ with the same direction of $\boldsymbol{u}$ and $'$ as inlet and $''$ as outlet symbols.

According to eq. (2) a pressure rise in an axial impeller stage causes a change in the outflow $c_{A,u}'' \neq 0$ compared to the inlet conditions $c_{A,u}' = 0$. The second impeller, with an opposite direction of rotation, shall be designed without outlet swirl as there is already a swirl at the inlet $c_{B,u}' < 0$. Figure 1 represents the velocity components for a contra-rotating axial fan stage without outlet swirl $c_u'' = 0$.

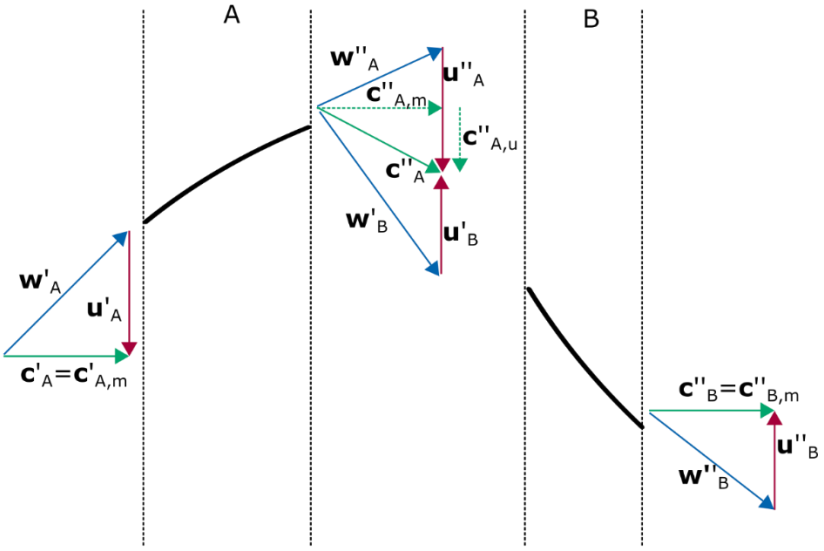

Figure 1: schematic representation of the velocity components

The fan configuration used in this paper corresponds to the schematic drawing as presented in Figure 2. Every impeller (A, B) is driven with a separate motor. Stationary components and rotating components are differently coloured. Stationary components are presented in black and rotating components are coloured in blue and red, according to the direction of rotation.

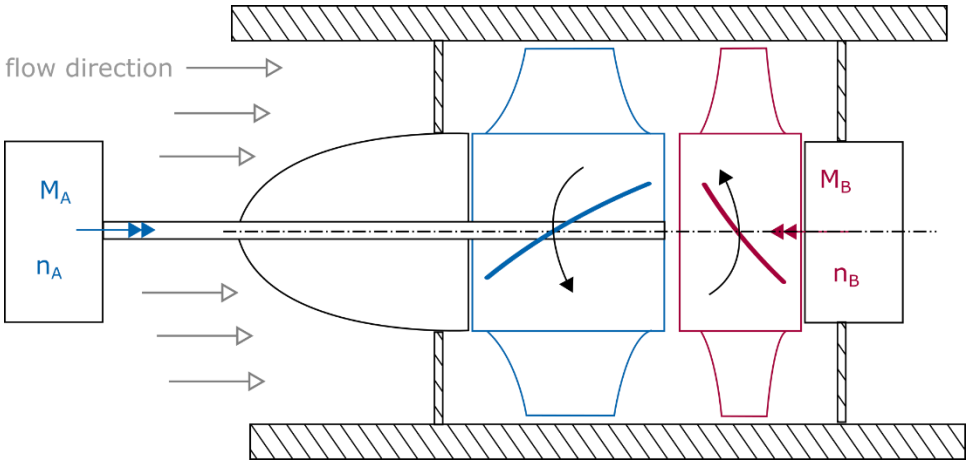

Figure 2: schematic representation of the construction

DESIGN PROCESS

The applied design process is modular both for each impeller but also within each impeller for different design steps. It takes the operating point and turbomachinery theory into account rather than pure geometric information.

The single impeller design is divided into the following steps:

1. Design point definition with total pressure rise as a ratio of the overall pressure difference, rotational speed of the impeller and direction of rotation (contra-rotating or not)
2. Definition of main dimensions consisting of hub and shroud diameter
3. Blade properties: setup of kinematics, definition of number of blades, definition of airfoil profiles plus stagger angle and chord length
4. 3d-generation of the blades by scaling and staggering the chosen airfoils and wrapping them onto their respective span's radius
5. If necessary sweeping of the blades by shifting the centre of gravity of each airfoil towards an acoustically beneficial position

According to step 1 the design of the CRF starts with the definition of the design point (Table 1) for both impellers. For the applied design approach only the gas density is needed as the flow can be considered as being incompressible and independent from the viscosity. The design point and the main dimensions according to step 2 are presented in Table 1.

Table 1: design point definition, main dimensions and dimensionless numbers

Parameter	Symbol	Unit	Impeller A	Impeller B	CRF
Flow rate	Q	m^3/s	0.15		
Total pressure difference	Δp_t	Pa	500	300	800
Speed	n	s^{-1}	133.3	83.3	105.4[1]
Air density	ρ	kg/m^3	1.2		
Hub-Diameter	D_H	m	0.080		
Shroud Diameter	D_S	m	0.12		
Flow coefficient	$\varphi = \frac{4Q}{\pi {D_S}^2 u}$[2]	--	0.26	0.42	0.33
Work coefficient	$\Psi = \frac{2\Delta p_t}{\varrho u^2}$	--	0.33	0.51	0.84
Diameter coefficient	$\delta = \frac{\Psi^{0.25}}{\varphi^{0.5}}$	--	1.48	1.30	1.66
Speed number	$\sigma = \frac{\varphi^{0.5}}{\Psi^{0.75}}$	--	1.18	1.08	0.66
Specific speed	$n_q = n\frac{Q^{1/2}}{\left(\frac{\Delta p_t}{\rho \cdot g}\right)^{3/4}}$	s^{-1}	3.10	2.84	1.72

The design of the blade properties by CFturbo is interactive. Initial settings are proposed by CFturbo and are based on latest turbomachinery design theory. To this end balance equations are solved together with the application of empirical co-relations. These co-relations are given with respect to the specific speed n_q, with g being the gravitational constant.

Different values are provided for information once the parameters have been chosen. This may be used to check and revise the draft of the fan during the interactive design. Also, based on the design point and impeller diameter, mid span estimations are provided for all velocity components (see Figure 3).

[1] $n_{CRF} = \sqrt{n_A\, n_B}$

[2] $u = \pi D_S n$

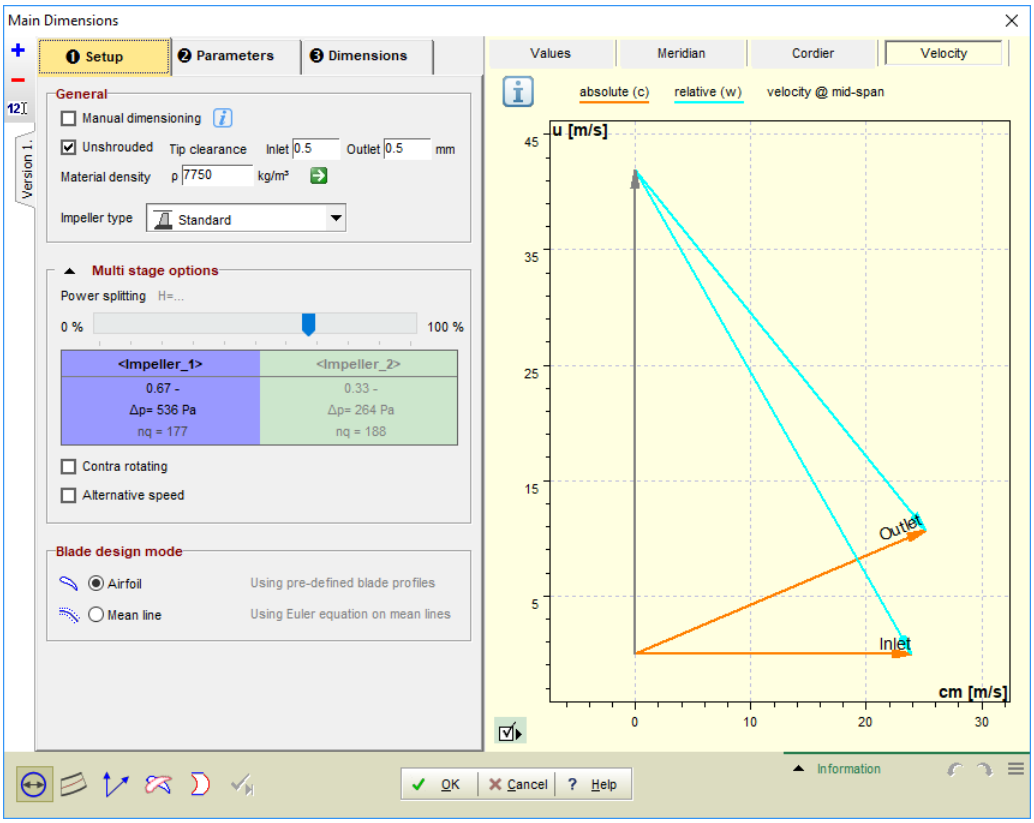

Figure 3: Main dimension of first impeller

Design step 3 is most important as it defines size and staggering of the blade profiles at each span. This determines the power transmission from the fan to the fluid. A beneficial post blade radial distribution of the absolute velocity components can be adjusted. Therefore a radial equilibrium is solved in CFturbo considering both the design point flow rate and the impeller's pressure difference at the design point.

Due to the high specific speed, a low-pressure fan has to be designed which leads the application of the blade element momentum theory, see e.g. [7]. A blade profile with aerodynamic properties relevant for the Reynolds-number scope in which the fan is to be operated was chosen (i.e. NACA 6508). Combining the above mentioned absolute velocity component distribution and the aerodynamic properties (lift and drag coefficient) of the airfoil within the blade element momentum theory yields suggestions for a reasonable set of stagger angle and chord length for each span of the blade.

All design steps shall be done for both impellers. The complete geometric representation of the fan is parametric. This allows for an entire 3D-geometry update if one of these previously mentioned parameters is changed. The CRF obtained using CFturbo is displayed in Figure 4.

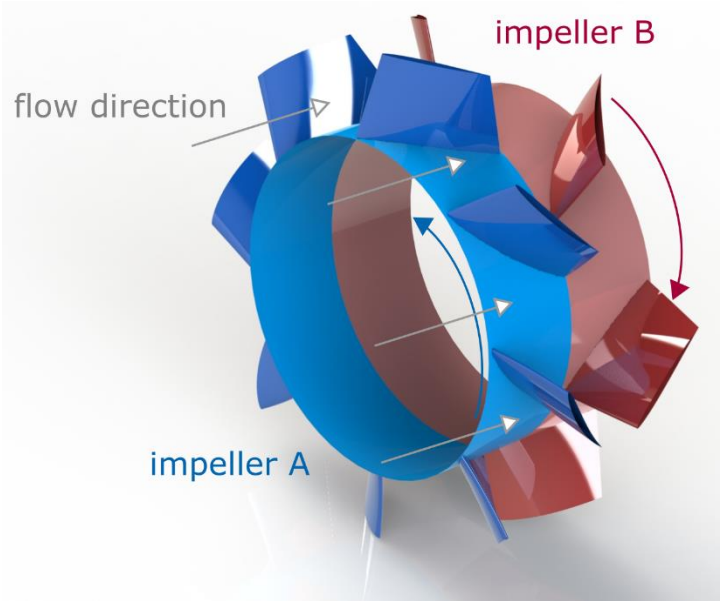

Figure 4: 3D geometry of the fan

MEASUREMENT SET-UP

Performance test

The measurement of the technical parameters is obtained using a test rig according to DIN EN ISO 5801 [3]. The test rig, presented in Figure 5, consists of a volume flow measurement (1) according to DIN EN ISO 5167-2 [4], a supply fan (2) with throttle (3) succeeded by a suction-sided pressure-measurement chamber with rectifiers (4). The impeller A (9) is driven by a motor (5) via a drive shaft (6) with torque measurement (7). The impeller B (11) is driven by a second motor (12). Both impellers are mounted on hubs with a spinner (9) at the inlet nozzle (8).

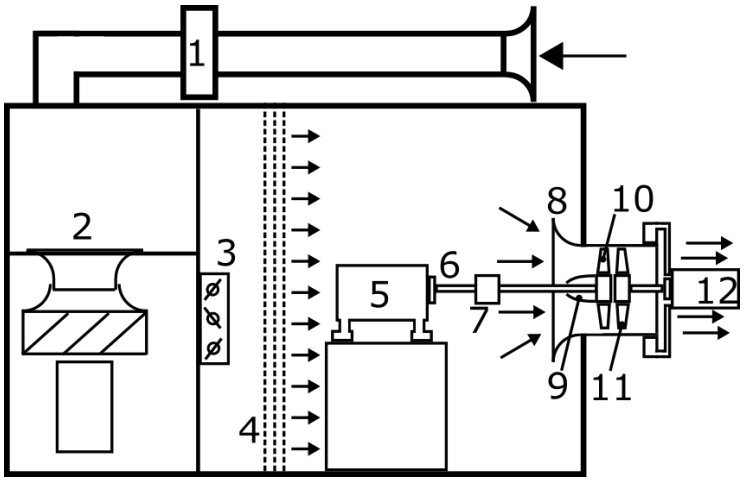

Figure 5: schematic representation of the test rig according to DIN EN ISO 5801

The rack with the installed fan is presented at left hand in Figure 6. The right hand side demonstrates the view at pressure side of the test chamber with integrated CRF.

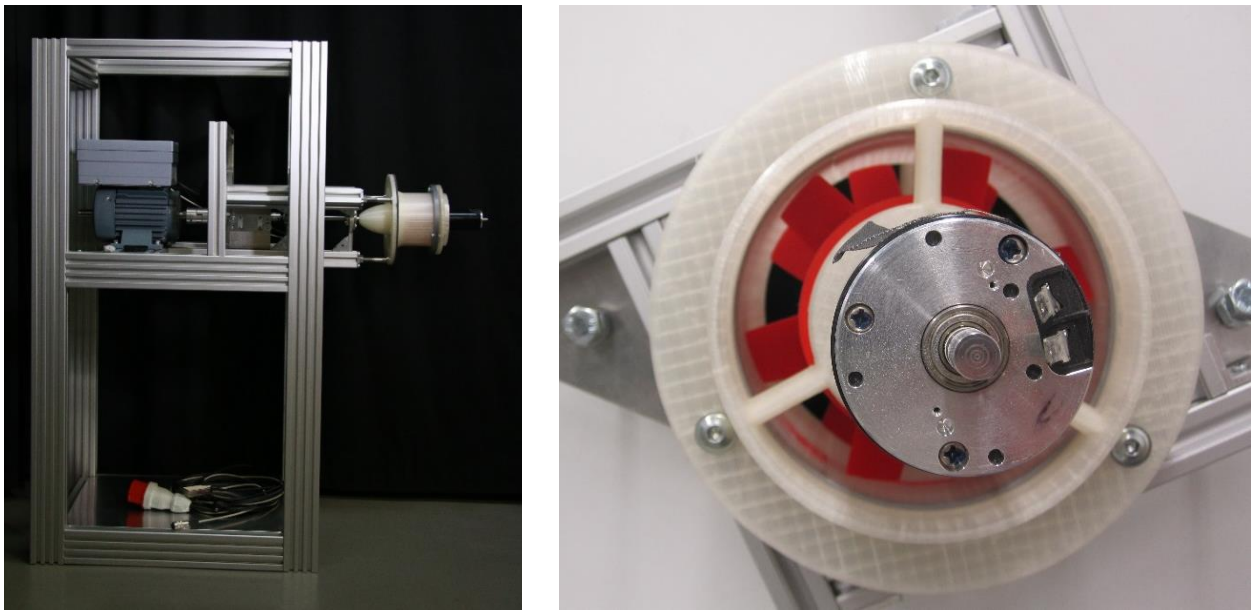

Figure 6: first stage of the contra-rotating fan mounted in a rack and view at pressure side of the test chamber

Investigation of the velocities

The velocity distribution at the fan outlet is measured using Particle-Image-Velocimetry (PIV). PIV uses light-reflecting particles like aerosols added to fluid. The particles are illuminated by a thin light sheet. The reflection distribution is captured at two different time steps with a camera normally orientated to the light sheet. Comparing both pictures with a convenient correlation method provides both vector components of movement for all particle-assemblies in the picture and within the plain illuminated with the light sheet.

The third velocity component can be obtained by taking a second camera and arranging both cameras at the certain angle to the light sheet. This set-up is called Stereo-Particle-Image-Velocimetry.

The experimental setup and the schematic drawing are presented in Figure 7. Laser (L) and cameras (C1, C2) are mounted on a three-axis-traverse. The laser illuminates the outlet of the fan (CRF) normal to the outlet opening. The area under investigation can be adjusted by using the traverse.

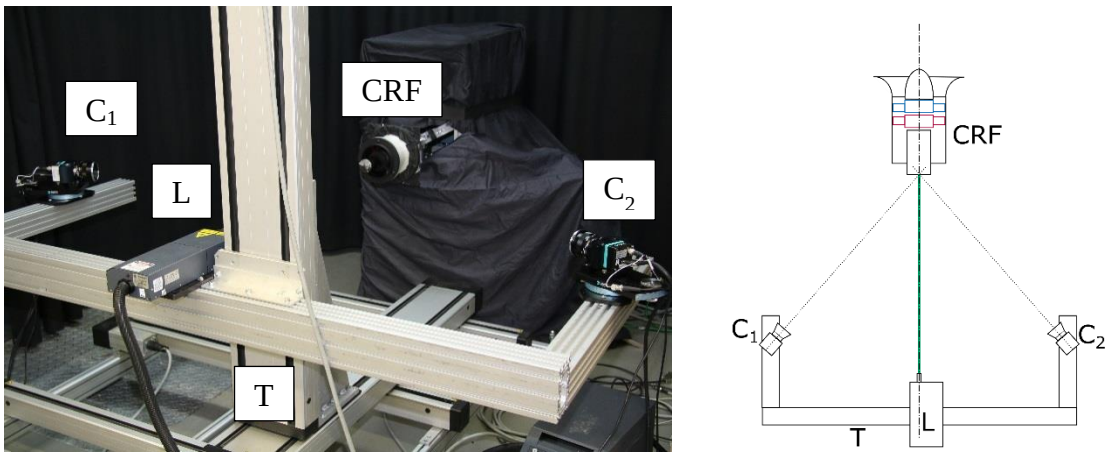

Figure 7: experimental setup for outlet velocity measurement using particle image velocimetry (left) and schematic drawing (right)

It shall be remarked, that upon high reflections caused by impeller B the velocity profile is measured 60 mm downstream the fan's outlet.

RESULTS

Performance test

The results obtained by the performance tests are presented in Figure 8 and Figure 9. The speed ratio is given as parameter $\frac{n_A}{n_{CRF}} : \frac{n_B}{n_{CRF}}$. The measurements have been carried according to Table 2. The same symbols and definitions are used in the subsequent sections.

Table 2: measured configurations

No.	n A 1/s	n B 1/s	Speed ratio	Sign
1	105,0	100	1,02:0,98	×
2	133,3	83,3	1,26:0,79	□
3	133,3	91,7	1,21:0,83	○
4	133,3	100	1,15:0,87	Δ

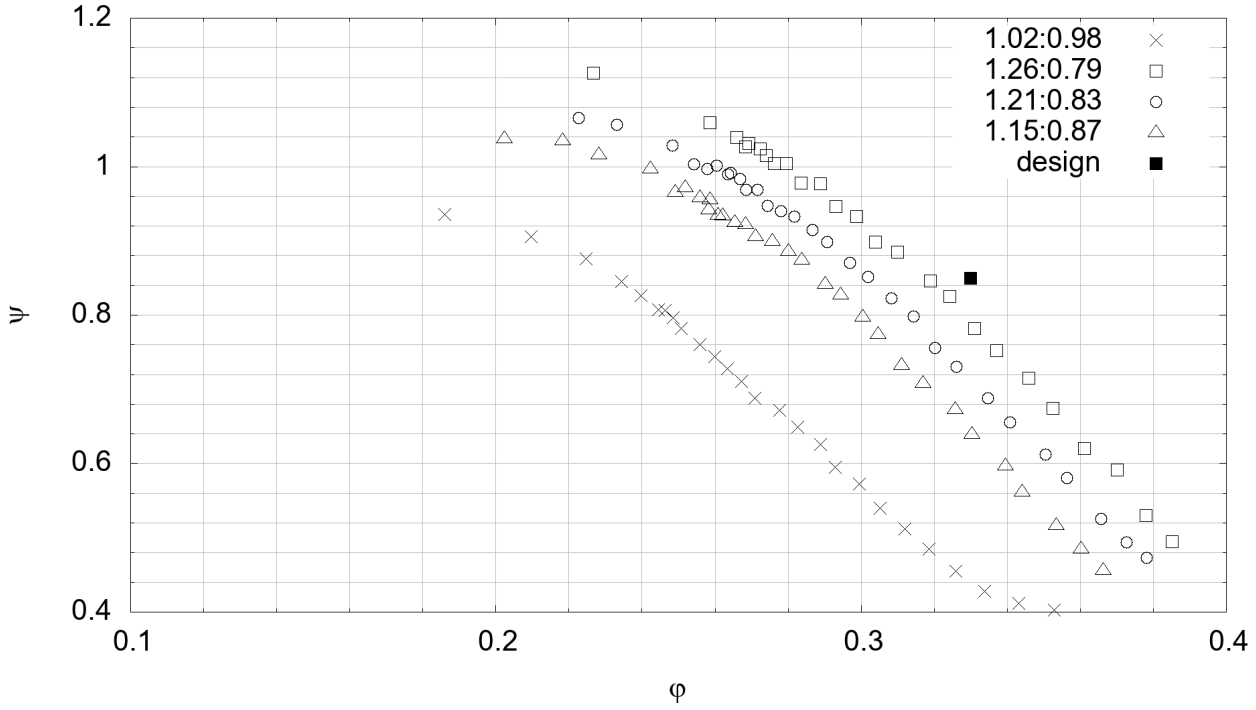

Figure 8: Work coefficient vs. flow coefficient for a contra-rotating stage of impeller A and impeller B. The parameter curves are representing different speed ratios between A and B

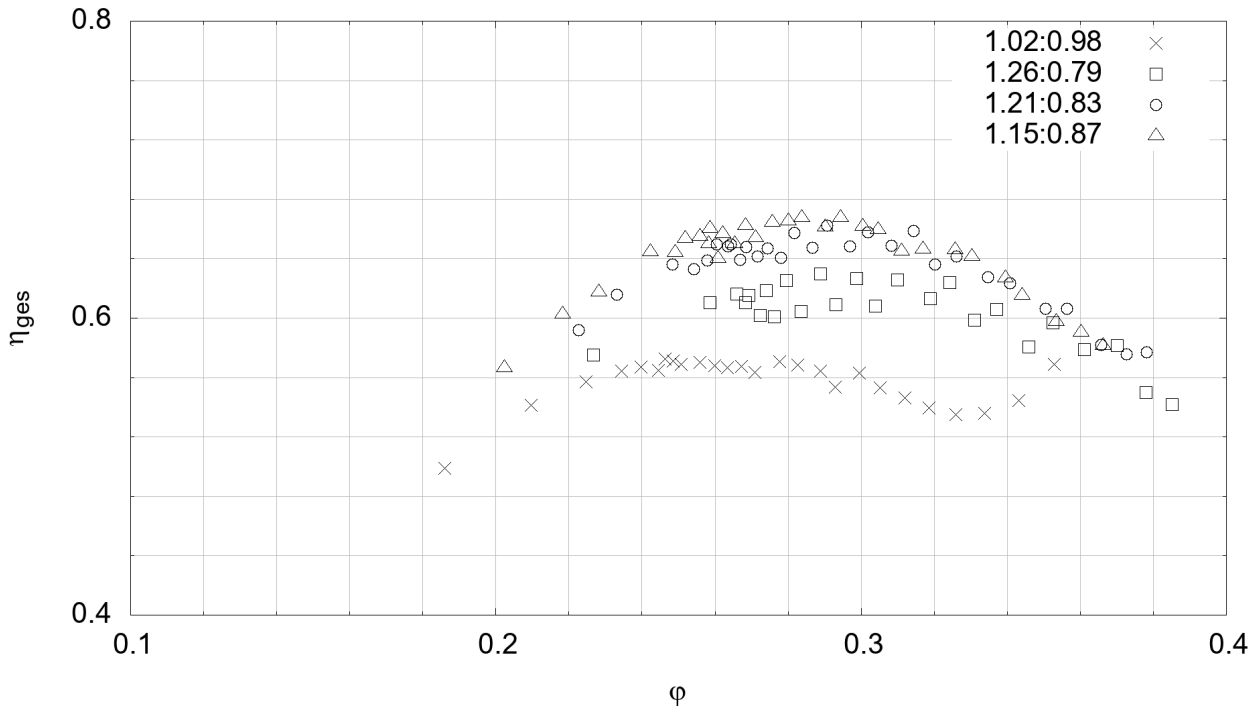

Figure 9: Total efficiency vs. flow coefficient for a contra-rotating stage of impeller A and impeller B. The parameter curves are representing different speed ratios between A and B

As presented in Figure 8 the design point fits the measured values sufficiently. According to Figure 9, the highest efficiency $\eta_{ges} = \frac{Q\,\Delta p_t}{(2\pi\, n_A M_A)+(P_B)}$ is obtained at a flow coefficient φ_{opt}= 0.29, wherein M_A indicates the measured momentum for impeller A and P_B the measured power input for impeller B. The optimum speed ratio within the measured range is 1.15:0.87, with the corresponding work coefficient $\Psi_{opt} = 0.84$.

For the CRF under investigation the maximum efficiency increases with decreasing speed difference between n_A and n_B. The subsequent velocity measurements shall show the dependency of the velocity profile at the fan's outlet on the speed ratio.

Investigation of the velocities

The velocity profile obtained using Stereo-PIV is presented in Figure 10. The velocity is represented as the ratio of the velocity component and the absolute velocity value $c = |\boldsymbol{c}|$. It can be stated that the peripheral velocity component c_u is depending upon the speed ratio, whilst having a constant axial component c_m. Also, the component in radial direction c_r is independent from the speed ratio and shall be neglected in further considerations.

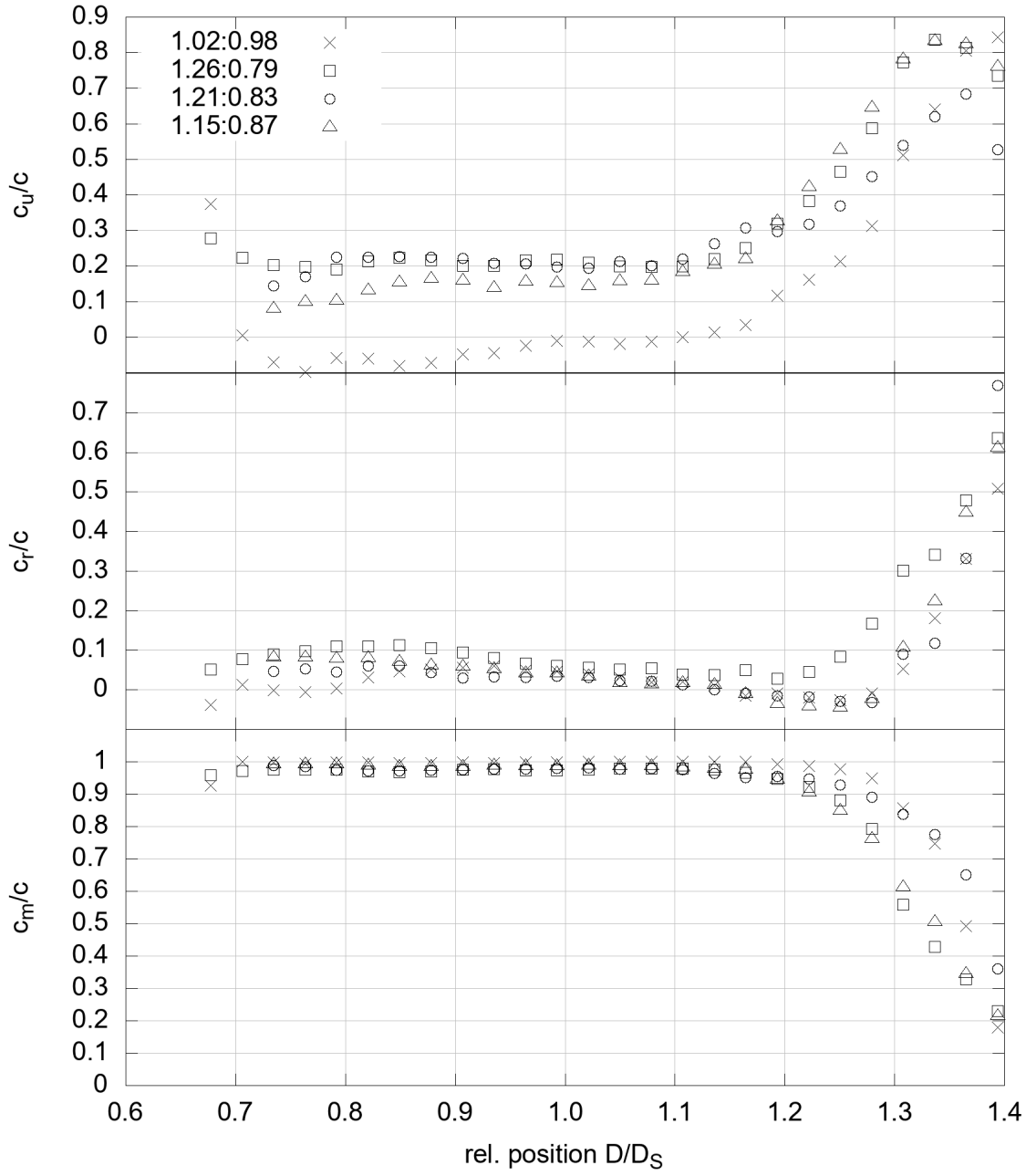

Figure 10: relative velocity profile by means of PIV for different rotational speed ratios

The design point (1.26:0.79) does not meet the swirl-free condition in this case. The swirl free condition is obtained at the ratio 1.02:0.98. The reasons for this differences shall be investigated in further steps. One reason is probably the setup of the correct point of operation during PIV-measurements in comparison to the performance measurement. Nevertheless, the function principle of the fan has been proved.

CONCLUSION

The design and the performance parameters as well as the outlet velocity distribution have been presented meeting the requirements for a small and compact contra-rotating axial fan.

The swirl at the CRF's outlet depends upon the rotational speed correlation between both impellers and can be eliminated. A swirl-free outlet flow is needed for subsequent components, like heat exchanger and filters, and will increase the performance of these devices.

The analytical design approach using CFturbo meets the required parameters, but further investigations are needed to yield a better understanding of the underlying effects for the transient fluid-impeller interaction, leading to an increased hit-ratio of the parameter efficiency and a swirl-free outlet condition.

The measurement of the fan performance and the velocity field at the outlet verifies the correlation between efficiency and the peripheral velocity. By decreasing c_u, the performance measurement provides an increase in η_{ges}.

The correlation between the peripheral velocity component and the fan's efficiency proves the necessity of controlling the swirl- free outlet condition. Especially in case of changing air duct pressure drop in time, an adjustment of the speed ratio between impeller A and B is required.

As a side remark it shall be mentioned that the definition of the representative rotational speed for the CRF $n_{CRF} = \sqrt{n_A\, n_B}$ is not in agreement with the performance measurement results. A more appropriate definition should be used in further investigations.

ACKNOWLEDGEMENTS

The authors would like to thank Mr. Konrad Friedrich and Mr. Phil Bender for their contributions to the measurements. The research project is funded by the German Federal Ministry of Economic Affairs and Energy (BMWi) under the title "*Mehrstufiger gegenläufiger Axialventilator mit automatischer betriebspunktunabhängiger Drallvermeidung* (Multi-stage contra-rotating axial fan with automatic operating point-independent swirl avoidance)" (MF150057).

Supported by:

Federal Ministry
for Economic Affairs
and Energy

on the basis of a decision
by the German Bundestag

BIBLIOGRAPHY

[1] M. Heinrich, Ch. Friebe, F. Bothe, R. Schwarze – *Experimental and numerical investigation of a gearless one-motor contra-rotating fan.* Journal of Power and Energy, 1-10, **2016**

[2] F. Bothe, Ch. Friebe, M. Heinrich, R. Schwarze – *CFD-Simulation of isothermal Turbomachinery - A Comparison of Results from ANSYS FLUENT and OPENFOAM* ASME Turbo Expo 2014: Power for Land, Sea and Air, GT2014, Düsseldorf, 2014, **2014**

[3] DIN EN ISO 5801 – *Industrial fans – Performance testing using standardized airways (ISO 5801:2007, including Cor 1:2008);German version EN ISO 5801,* **2008**

[4] DIN EN ISO 5167-2 –*Measurement of fluid flow by means of pressure differential devices inserted in circular-cross section conduits running full – Part 2 Orifice plates (ISO 5167-2:2003;German version EN ISO 5167-2,* **2008**

[5] F. Berlage – *Ein Windkanal mit zwei gegenläufigen Luftschrauben.* Luftfahrt und Schule, S. 178 **1936**

[6] W. Traupel – *Versuche an einem gegenläufigen Axialventilator*. Heiz.-Lüft.-Haustechnik Vol. 10, Nr. 1, **1959**

[7] T. Carolus – *Ventilatoren, Aerodynamischer Entwurf, Schallvorhersage, Konstruktion.* 3. Auflage Springer Vieweg, **2012**

[8] E. B. Bell, L. J. DeKoster – *Test of a dual-rotation axial-flow fan*. Langley Memorial Aeronautical Laboratory, NACA Library, L-303, 1942

[9] H. Nouri, F. Ravelet, F. Bakir, C. Sarraf, R. Rey – *Design and Experimental Validation of a Ducted Counter-rotating Axial-flow Fans System*, Journal of Fluid Engineering, 134(10), **2012**

[10] C. Mistry, A.M. Pradeep – *Experimental investigation of a high aspect ratio, low speed contra-rotating fan stage with complex inflow distortion*. Propulsion and Power Research, vol.3, no. 2, pp. 68 - 81, **2014**

[11] D.S. Pundhir, P.B. Sharma – *A Study of Aerodynamic Performance of a Contra-Rotating Axial Compressor Stage*. Defence Science Journal, vol. 42, no. 3, pp 191-199, **1992**

[12] CFturbo GmbH, – *CFturbo Version 10.3*, **2017**